



## Research Article

# A Highly Sensitive and Selective Colorimetric $\text{Hg}^{2+}$ Ion Probe Using Gold Nanoparticles Functionalized with Polyethyleneimine

Kyung Min Kim <sup>1,2</sup>, Yun-Sik Nam,<sup>3</sup> Yeonhee Lee,<sup>3</sup> and Kang-Bong Lee <sup>1</sup>

<sup>1</sup>Green City Technology Institute, Korea Institute of Science and Technology, Hwarang-ro 14 gil 5, Seoul 02792, Republic of Korea

<sup>2</sup>Department of Chemistry, Korea University, Anam-ro, Seongbuk-gu, P.O. Box 145, Seoul 136-701, Republic of Korea

<sup>3</sup>Advanced Analysis Center, Korea Institute of Science and Technology, Hwarang-ro 14 gil 5, Seoul 02792, Republic of Korea

Correspondence should be addressed to Kang-Bong Lee; leekb@kist.re.kr

Received 11 October 2017; Revised 6 December 2017; Accepted 18 December 2017; Published 5 February 2018

Academic Editor: Silvana Andreescu

Copyright © 2018 Kyung Min Kim et al. This is an open access article distributed under the Creative Commons Attribution License, which permits unrestricted use, distribution, and reproduction in any medium, provided the original work is properly cited.

A highly sensitive and selective colorimetric assay for the detection of  $\text{Hg}^{2+}$  ions was developed using gold nanoparticles (AuNPs) conjugated with polyethyleneimine (PEI). The  $\text{Hg}^{2+}$  ion coordinates with PEI, decreasing the interparticle distance and inducing aggregation. Time-of-flight secondary ion mass spectrometry showed that the  $\text{Hg}^{2+}$  ion was bound to the nitrogen atoms of the PEI in a bidentate manner (N– $\text{Hg}^{2+}$ –N), which resulted in a significant color change from light red to violet due to aggregation. Using this PEI-AuNP probe, determination of  $\text{Hg}^{2+}$  ion can be achieved by the naked eye and spectrophotometric methods. Pronounced color change of the PEI-AuNPs in the presence of  $\text{Hg}^{2+}$  was optimized at pH 7.0, 50°C, and 300 mM NaCl concentration. The absorption intensity ratio ( $A_{700}/A_{514}$ ) was correlated with the  $\text{Hg}^{2+}$  concentration in the linear range of 0.003–5.0  $\mu\text{M}$ . The limits of detection were measured to be 1.72, 1.80, 2.00, and 1.95 nM for tap water, pond water, tuna fish, and bovine serum, respectively. Owing to its facile and sensitive nature, this assay method for  $\text{Hg}^{2+}$  ions can be applied to the analysis of water and biological samples.

## 1. Introduction

Mercury ion ( $\text{Hg}^{2+}$ ) is ubiquitously distributed in the environment, and it is considered to be one of the major environmental pollutants to be widely used in industry, agriculture, and medicine. It is nonessential and toxic to the human body.  $\text{Hg}^{2+}$  is considered to be one of the major environmental pollutants to be widely used in industry, agriculture, and medicine. This mercury ion exists in inorganic and organic mercury ions. Upon entering the body, inorganic mercury ions are accumulated mainly in the kidneys and give rise to vomiting and diarrhea, followed by hypovolemic shock, oliguric renal failure, and possibly death [1–4]. Organic mercury ions such as methylmercuric ( $\text{MeHg}^+$ ), ethylmercuric ( $\text{EtHg}^+$ ), and phenylmercuric ( $\text{PhHg}^+$ ) ions can also cause injuries at the central nervous system and lead to paresthesias, headaches, ataxia, dysarthria, visual field constriction, blindness, and hearing impairment [5–7]. Therefore, detection of mercury ion in various sample matrices has been an urgent issue.

Several analytical techniques, such as direct mercury analyzer (DMA) [8], ion chromatography (IC) [9], and high performance liquid chromatography (HPLC) [10, 11], have been utilized to detect mercury ions. However, these ways generally require complicated sample pretreatment process, skillful technicians, and sophisticated instrumentations. Therefore, the low-cost and facile analytical method for selective detection of mercury ions remains to be a challenge for analytical chemists.

Various nanoparticle assays for a simple detection of  $\text{Hg}^{2+}$  ions have recently been investigated using gold nanorods (AuNRs) [12], carbon nanoparticles (CNPs) [13], silver nanoparticles (AgNPs) [14], silver nanoprisms (AgNPRs) [15], and AuNPs [16–18]. These colorimetric methods are especially promising in the analysis of  $\text{Hg}^{2+}$  with their naked eye or UV-Vis applications, due to their high extinction coefficients and the interparticle distance-dependent optical properties.

Polyethyleneimine (PEI) was applied to use a chemical functionalizer as a harmless gene delivery mediator, templates, stabilizers, and molecular gum to arrange metal nanoparticles

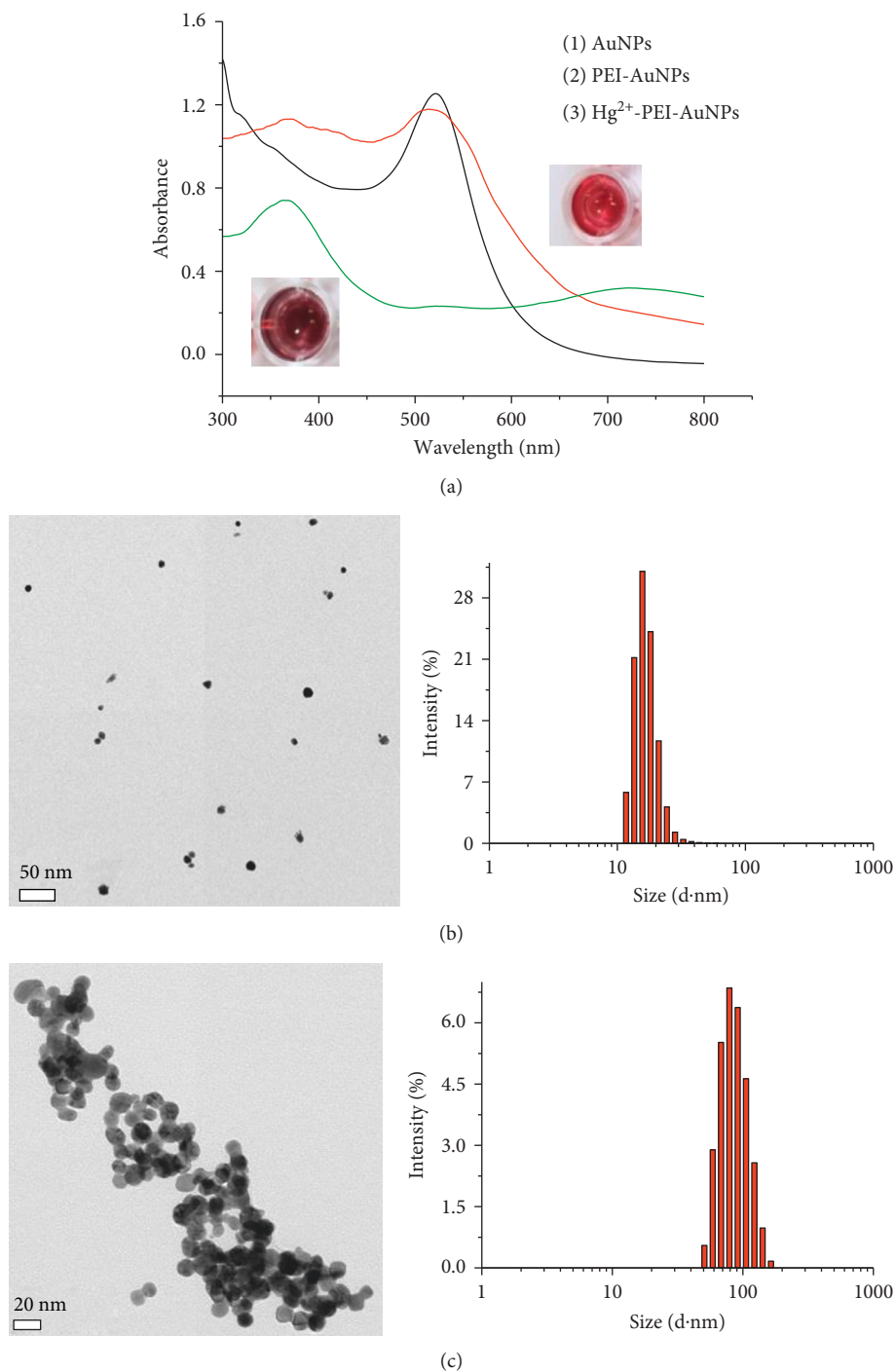


FIGURE 1: (a) UV-Vis absorption spectra of (1) AuNPs (black line), (2) PEI-AuNPs (red line), and (3) PEI-AuNPs conjugated with Hg<sup>2+</sup> (green line). (b) TEM image of PEI-AuNPs (left) and the corresponding particle-size distribution histogram (right). (c) TEM image of PEI-AuNPs conjugated with Hg<sup>2+</sup> (left) and particle-size distribution histogram (right).

[19–22]. Various amine groups could give sufficient active sites for strong combining capability, and these characteristics of PEI can be useful to control the selectivity of different ions. For its application, AuNPs conjugated with PEI (PEI-AuNPs) have been utilized as delivery of drug and gene in breast cancer therapy [23].

This study showed that PEI-AuNPs were aggregated with inorganic and organic mercury ions, and these ions induced the definite color change of AuNPs selectively among other

diverse ions. Dispersed and aggregated AuNPs were characterized by ultraviolet-visible spectroscopy (UV-Vis), high-resolution transmission electron microscopy (HR-TEM), and dynamic light scattering (DLS) upon addition of Hg<sup>2+</sup>. Hg<sup>2+</sup> ion binding sites on the surface of PEI-AuNPs were elucidated by <sup>13</sup>C nuclear magnetic spectroscopy (<sup>13</sup>C NMR), X-ray photoelectron spectroscopy (XPS), and time-of-flight secondary ion mass spectrometry (TOF-SIMS) [24, 25]. The

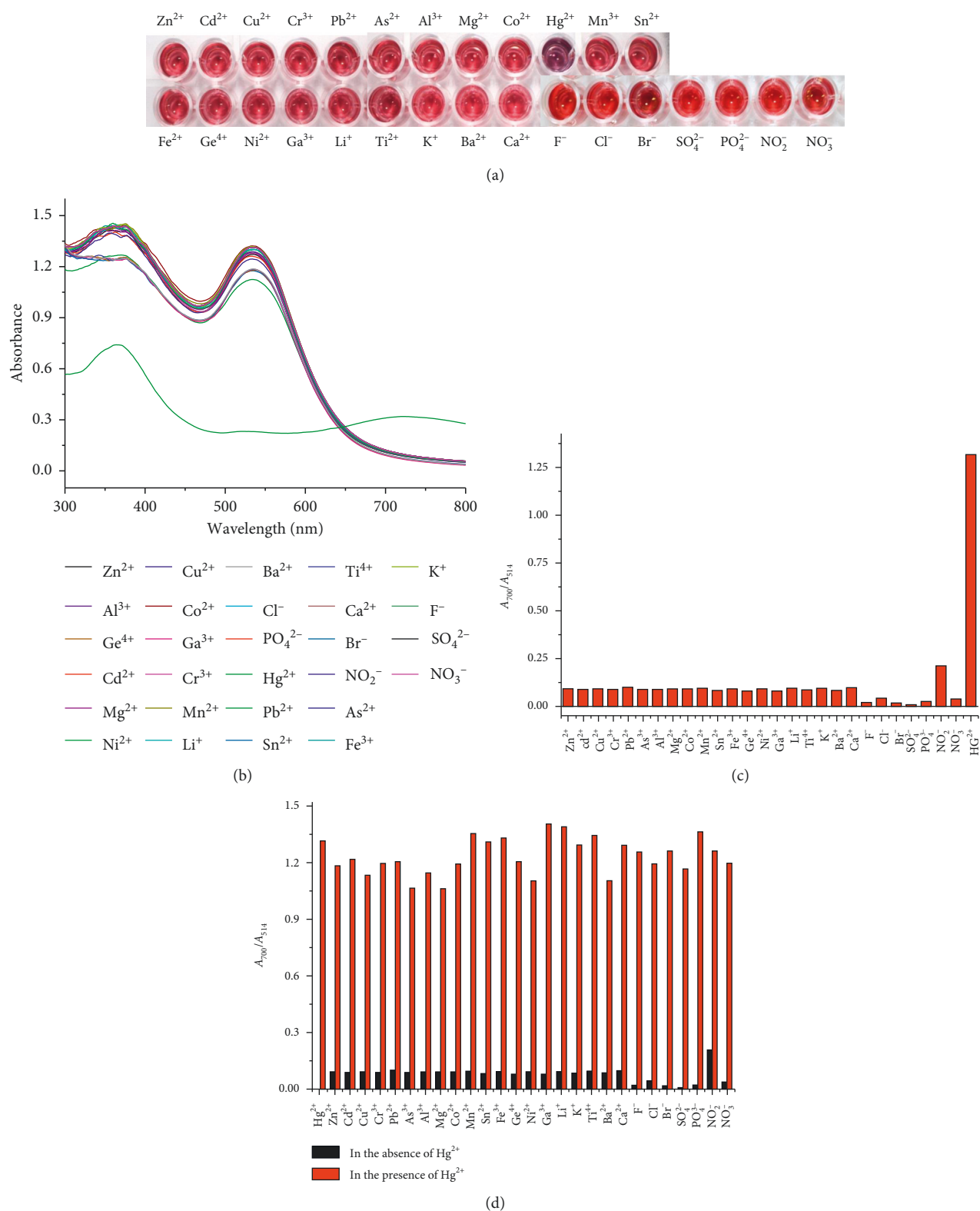


FIGURE 2: (a) Photographic images, (b) UV-Vis absorption spectra, (c) absorption ratios ( $A_{700}/A_{514}$ ) of PEI-AuNPs with  $5.0 \mu\text{M} \cdot \text{Hg}^{2+}$  ion and  $50 \mu\text{M}$  various ions at pH 7,  $50^\circ\text{C}$ , and  $500 \text{ mM} \cdot \text{NaCl}$  concentration, and (d) absorption ratios ( $A_{700}/A_{514}$ ) of PEI-AuNPs with  $50 \mu\text{M}$  various ions in the presence and absence of  $5.0 \mu\text{M} \cdot \text{Hg}^{2+}$ .

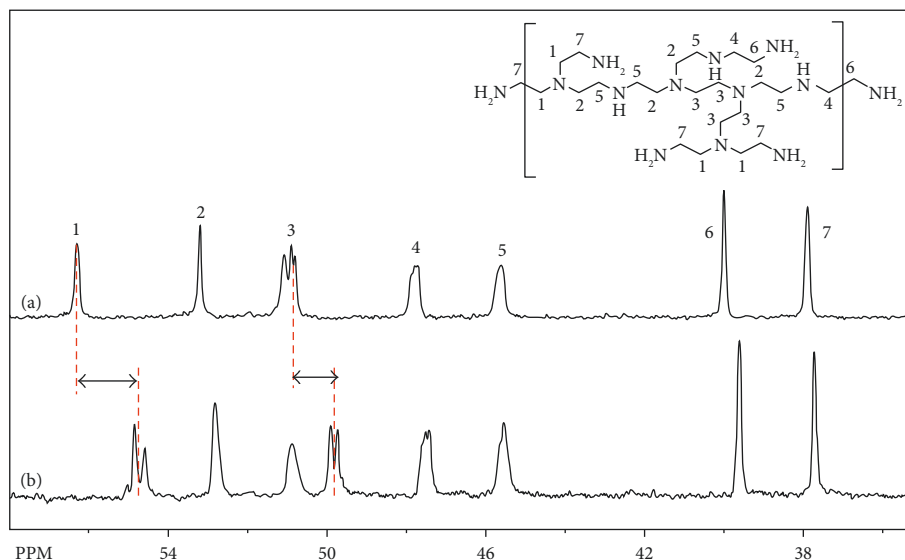


FIGURE 3:  $^{13}\text{C}$  NMR spectra for (a) PEI and (b) PEI-AuNPs in  $^2\text{H}_2\text{O}$  at room temperature.

interference effects were tested in the presence of other metal ions and anions. Also, PEI-AuNP assay method for detection of  $\text{Hg}^{2+}$  ion was optimized in terms of pH, temperature, and salt condition.

This present assay using PEI-AuNP was very simple, cost-efficient, and allowed for the on-site detection of  $\text{Hg}^{2+}$  in real time. The limit of detection (LOD) was  $\sim 2$  nM in various samples. Therefore, this technique could be utilized to monitor  $\text{Hg}^{2+}$  ions in a wide range of practical samples.

## 2. Experimental

**2.1. Materials.** Gold (III) chloride trihydrate ( $\text{HAuCl}_4 \cdot 3\text{H}_2\text{O}$ ), PEI, methylmercuric chloride, and phenylmercuric chloride were sourced from Sigma-Aldrich (St. Louis, MO, USA). Ethylmercuric chloride was obtained from Chem Service (Tower Lane, West Chester, USA). Salts of  $\text{NO}_3^-$ ,  $\text{NO}_2^-$ ,  $\text{PO}_4^{3-}$ ,  $\text{SO}_4^{2-}$ ,  $\text{Br}^-$ ,  $\text{Cl}^-$ ,  $\text{F}^-$ ,  $\text{Ca}^{2+}$ ,  $\text{Cd}^{2+}$ ,  $\text{Fe}^{3+}$ ,  $\text{Ba}^{2+}$ ,  $\text{Mn}^{2+}$ ,  $\text{Ga}^{3+}$ ,  $\text{Ti}^{4+}$ ,  $\text{Al}^{3+}$ ,  $\text{Mg}^{2+}$ ,  $\text{K}^+$ ,  $\text{Ge}^{4+}$ ,  $\text{Cr}^{3+}$ ,  $\text{Cu}^{2+}$ ,  $\text{Li}^+$ ,  $\text{As}^{3+}$ ,  $\text{Co}^{2+}$ ,  $\text{Sn}^{2+}$ ,  $\text{Pb}^{2+}$ ,  $\text{Hg}^{2+}$ ,  $\text{Ni}^{2+}$ , and  $\text{Zn}^{2+}$  were purchased from AccuStandard (New Haven, CT, USA). NaCl, HCl, and NaOH were purchased from Samchun Chemical (Gyeonggi-Do, Korea). Tap water was acquired from our laboratory and pond water was obtained from a pond at the Korea Institute of Science and Technology (KIST). Tuna fish was sourced from Dongwon (Seoul, Republic of Korea). Bovine serum was purchased from Sigma-Aldrich (St. Louis, MO, USA). Citrus leaf sample was obtained from Swan Leaf Pty Ltd (Perth, WA, Australia). Distilled water was obtained using a Milli-Q water purification system (Millipore, Bedford, MA, USA).

**2.2. Preparation of PEI-AuNPs.** PEI-AuNPs were synthesized as following literature procedures by mixing aqueous solutions of  $\text{HAuCl}_4 \cdot 3\text{H}_2\text{O}$  (1 mL, 0.025 M) and PEI (7.8 mL, 9.74 mM), with subsequent reduction of  $\text{HAuCl}_4$  at  $\sim$ pH 7.0 [26]. The mixture was kept to react for three days at ambient temperature, and  $\sim 10$  nm PEI-AuNPs were produced.

**2.3. Sample Preparation and  $\text{Hg}^{2+}$  Sensing Test Using PEI-AuNPs.** The suspended particles in all water samples were removed by a syringe filter ( $0.20 \mu\text{m}$  pore size) prior to analysis, and sample aliquots (9 mL) were mixed with a  $500 \mu\text{M} \cdot \text{Hg}^{2+}$  solution (1 mL) to produce a  $50 \mu\text{M} \cdot \text{Hg}^{2+}$  stock solution.

Tuna fish was obtained from a local supermarket. Its muscle tissues were crushed and dried on petri dishes overnight at  $85^\circ\text{C}$ . A small portion (ca. 0.3 g) was incubated in 2 mL  $\text{HNO}_3$  for 1 h before addition of 0.5 mL  $\text{HClO}_4$  (70%). Then, the samples were irradiated under a UV lamp for 3 h to convert all possibly contained organic mercury to inorganic mercury. Finally, the acid extracts were transferred to 50 mL volumetric flasks, and the volume was adjusted to 50 mL with Milli-Q water [27]. These samples were spiked with  $100 \mu\text{g} \cdot \text{mL}^{-1}$  of  $\text{Hg}^{2+}$ .

Stock solution of bovine serum was made to be 0.1% concentration in water. The suspensions were stirred and centrifuged alternately for 30 min and the solutions (9 mL) were blended with 1 mL of a  $100 \mu\text{g} \cdot \text{mL}^{-1}$   $\text{Hg}^{2+}$  solution.

0.9 g of citrus leaf was added to 5 mL concentrated  $\text{HNO}_3$  and heated for 2 h in the boiling water bath. After being cooled to room temperature, the samples were added with 2 mL of 30%  $\text{H}_2\text{O}_2$ , followed by heating for 1 h in the boiling water bath. Finally, the sample volume was made to 25 mL with double-distilled water. Before conducting experiments, the pH value of samples solution was neutralized by solid NaOH [28].

To evaluate the utility of our proposed method,  $\text{Hg}^{2+}$  concentrations added in tap, pond water, tuna fish, and bovine serum were measured with 1 mL of the PEI-AuNP solution, and followed by UV-Vis spectrophotometry. Those analytical results were confirmed with DMA.

**2.4. Instrumentation.** The absorption spectra were recorded by UV-Vis spectrophotometer (S-3100, Sinco, Seoul, Republic of Korea). UV-Vis spectra were acquired in the range

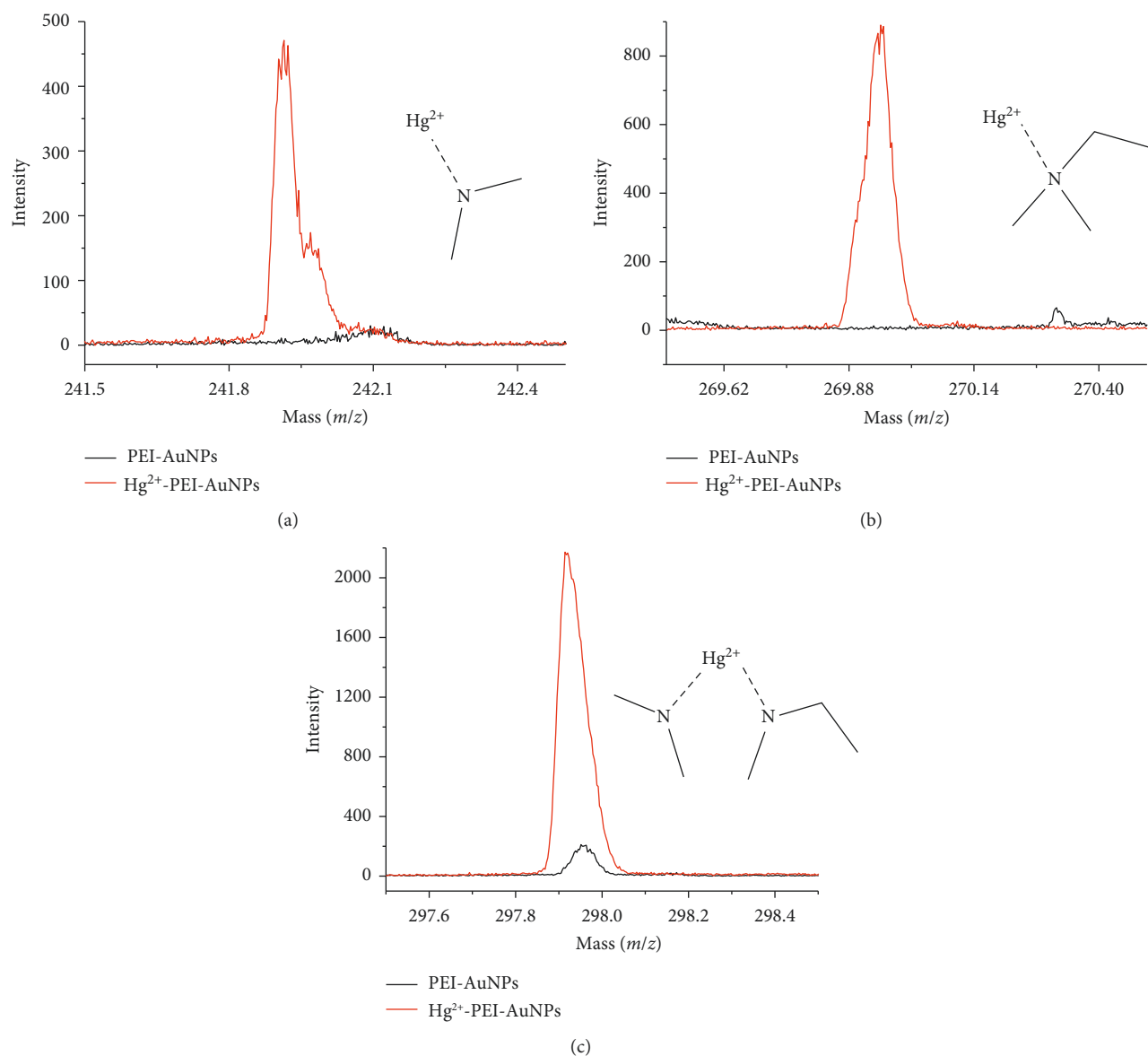


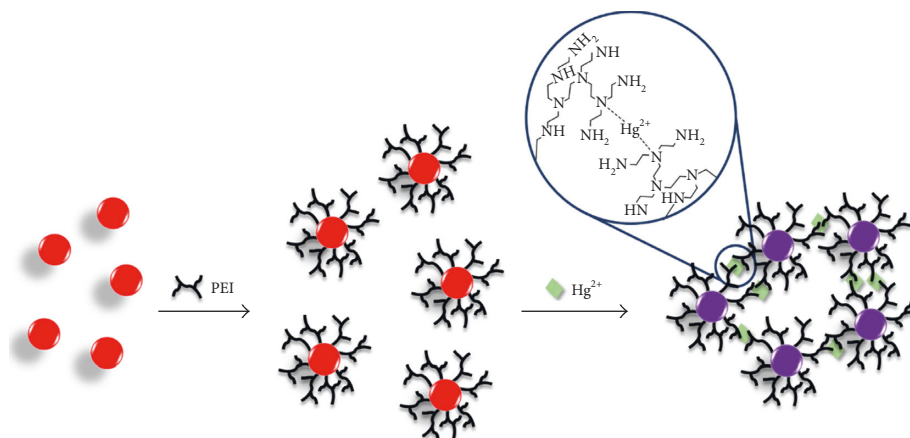
FIGURE 4: Mass peaks for (a)  $(\text{CH}_2)_2\text{NHg}^{2+}$  ( $m/z$ : 242), (b)  $\text{CH}_2\text{CH}_2(\text{CH}_2)_2\text{NHg}^{2+}$  ( $m/z$ : 270), and (c)  $(\text{CH}_2)_2\text{NHg}^{2+}\text{N}(\text{CH}_2)\text{CH}_2\text{CH}_2$  ( $m/z$ : 298) fragments in TOF-SIMS spectra of PEI-AuNPs (black) and PEI-AuNPs-Hg<sup>2+</sup> (red). These molecular fragments are expected based on PEI-AuNPs-Hg<sup>2+</sup> structural elements in the zoomed circle in Scheme 1.

of 300–800 nm by using 4 mm path length quartz cells. The pH measurements were conducted with an HI 2210 pH meter (Hanna Instruments, Woonsocket, RI, USA). The concentrations of Hg<sup>2+</sup> ions in various samples were measured by DMA (DMA 80, Milestone, Italy). <sup>13</sup>C NMR spectra were measured on an Avance III 400 MHz <sup>1</sup>H NMR spectrometer (Bruker, Billerica, MA, USA). XPS analysis was performed using a PHI 5000 VersaProbe III instrument (ULVAC-PHI, Chigasaki, Japan). Mass spectra were measured using TOF-SIMS (TOF-SIMS 5, ION-TOF, Münster, Germany). The size distributions of nanoparticles were recorded by a Zetasizer (Malvern Instruments Ltd., Worcestershire, UK). The images and sizes of PEI-AuNPs and their Hg<sup>2+</sup>-induced aggregates were measured on a micrograph using transmission electron microscope (TEM; CM30, Philips, NC, USA). TEM

samples were obtained by settling the scattered AuNPs and evaporating the solvent.

### 3. Results and Discussion

**3.1. Characterization of PEI-AuNPs and Their Complexes with Hg<sup>2+</sup>.** PEI-AuNPs were prepared as ~10 nm size as reducing HAuCl<sub>4</sub> with amine group of PEI. The AuNPs were usually synthesized by the citrate reduction of HAuCl<sub>4</sub>, and their sizes were ~33 nm as described in earlier studies [29], but AuNPs conjugated with PEI (PEI-AuNPs) under these conditions became much smaller. As a result, the mean AuNP size depended on the quantity and type of reducing agents, pH, temperature, and reaction time [30, 31]. A strong localized surface plasmon resonance (LSPR) peak of these



SCHEME 1: Schematic illustration of the AuNPs capped with PEI, and the aggregation of PEI-AuNPs reacted with Hg<sup>2+</sup> ion, accompanied by a color change, and the predicted coordination bond between Hg<sup>2+</sup> ions and PEI-AuNPs.

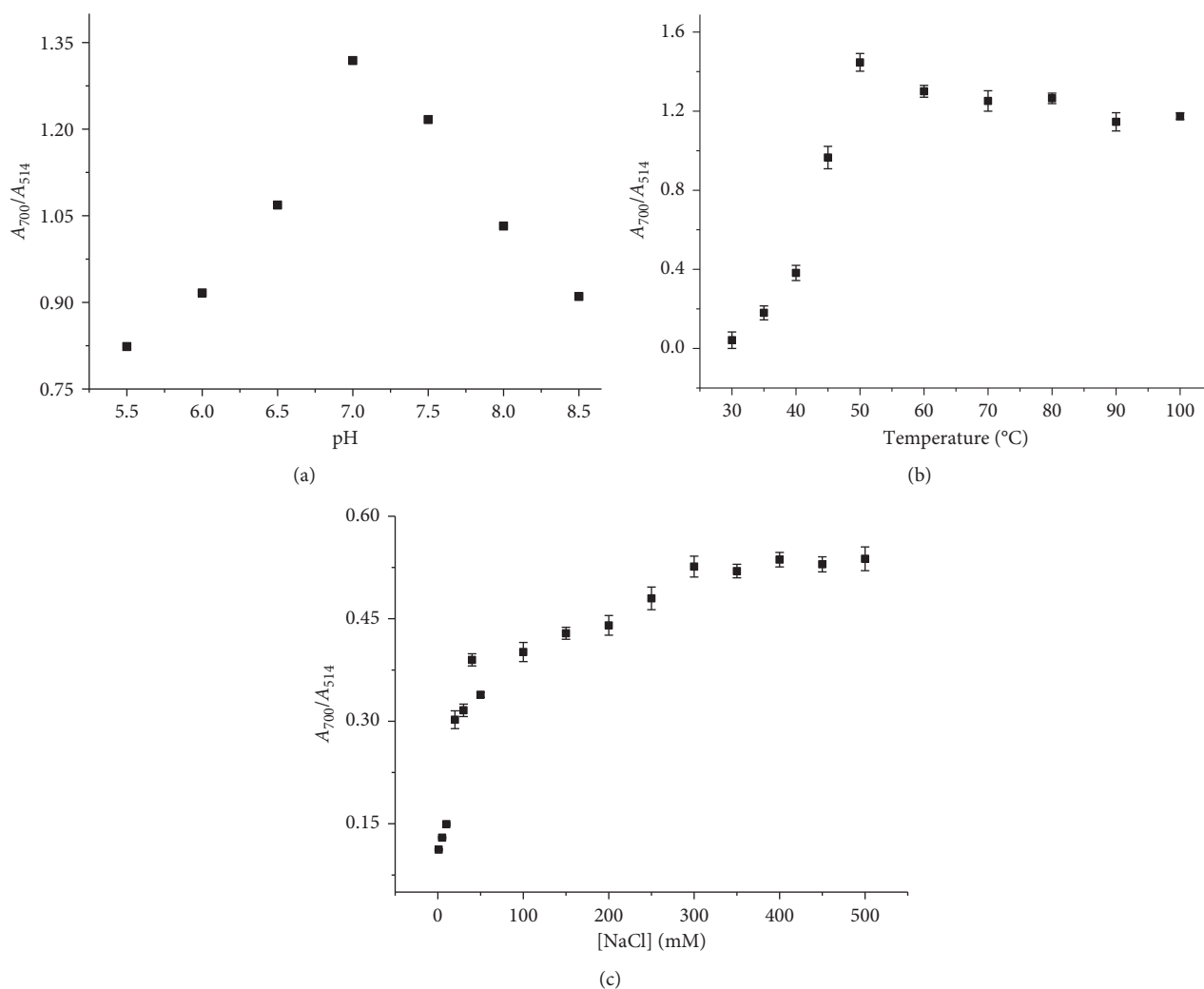
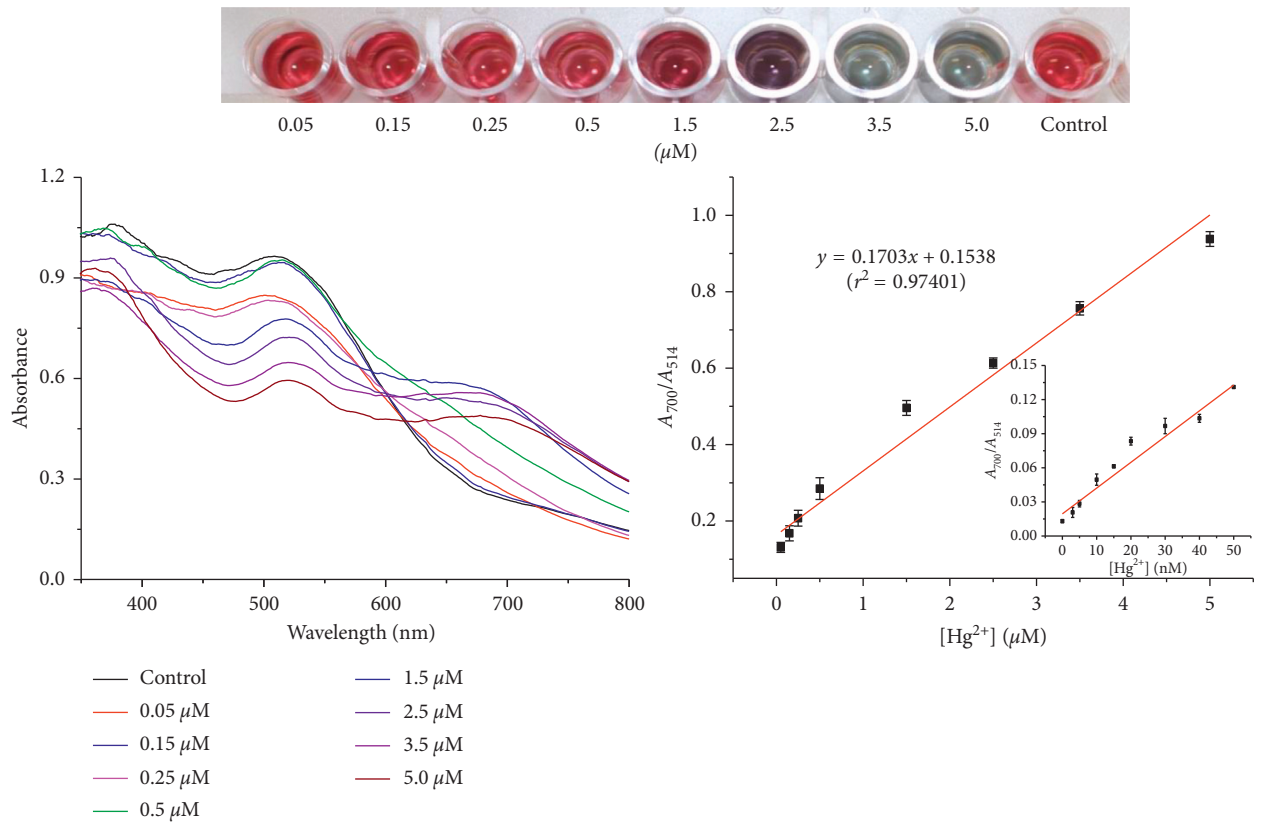


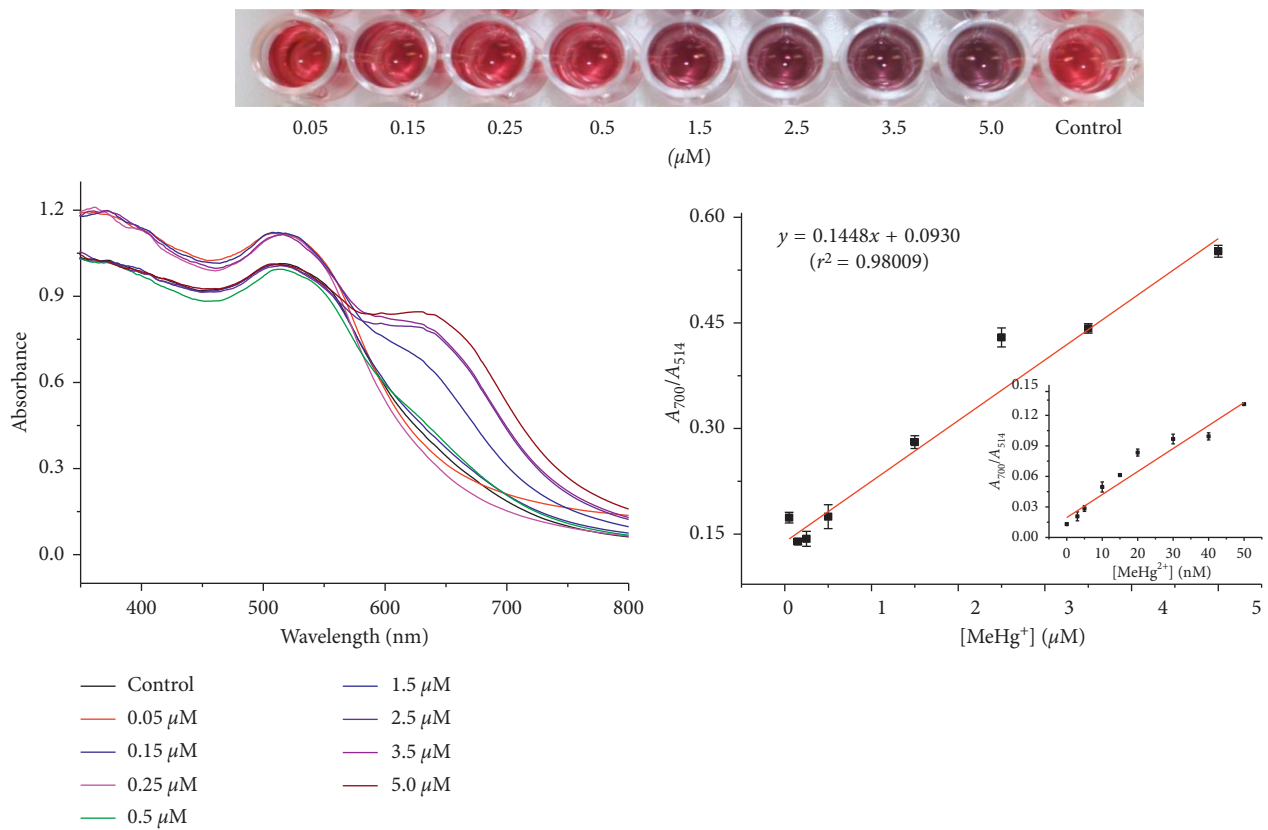
FIGURE 5: Absorption ratios ( $A_{700}/A_{514}$ ) of Hg<sup>2+</sup>-PEI-AuNPs as a function of (a) pH, (b) temperature, and (c) concentration of NaCl.

label-free AuNPs appeared at ca. 514 nm in their UV-Vis spectrum, resulting in the red color of the corresponding solution. The size of AuNPs influenced to change their

surface plasmon absorption maxima at 514 nm [32]. The sizes of PEI-AuNPs and Hg<sup>2+</sup>-PEI-AuNPs were distributed to be ~15 and ~75 nm, respectively, according to TEM



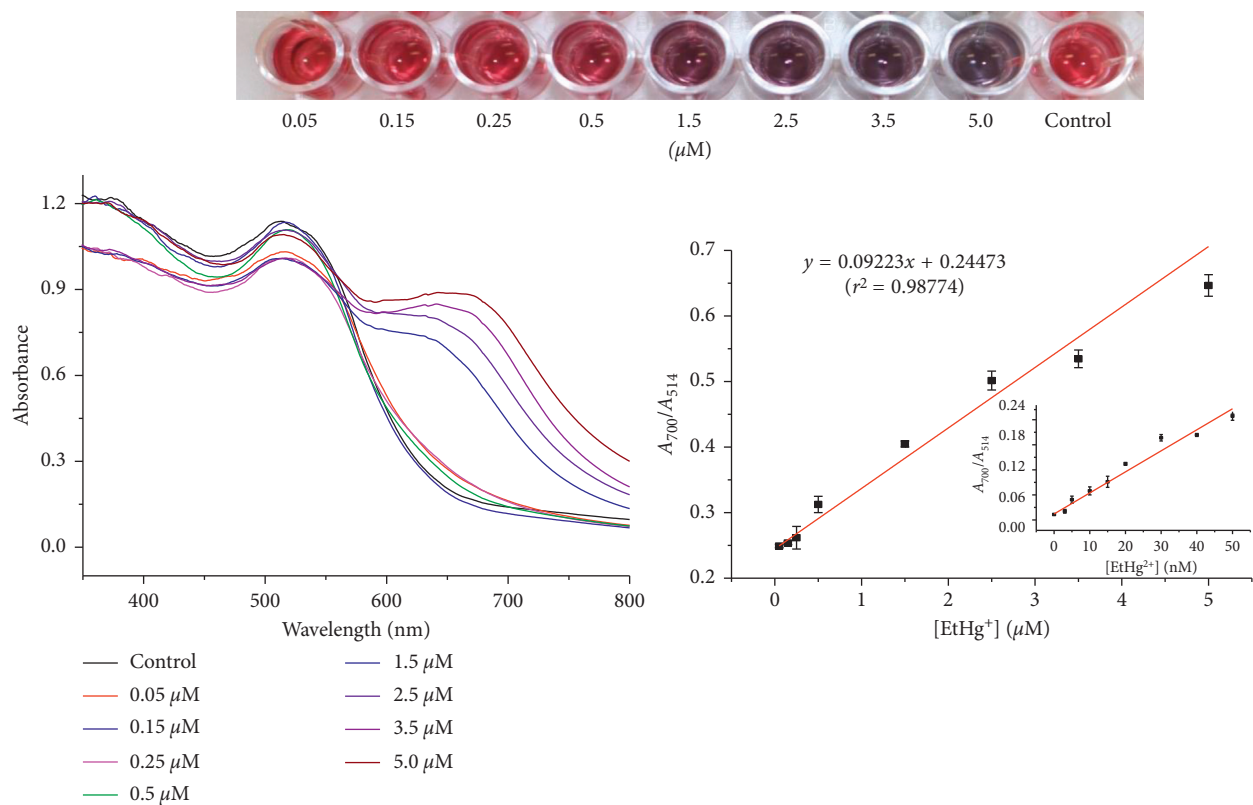
(a)



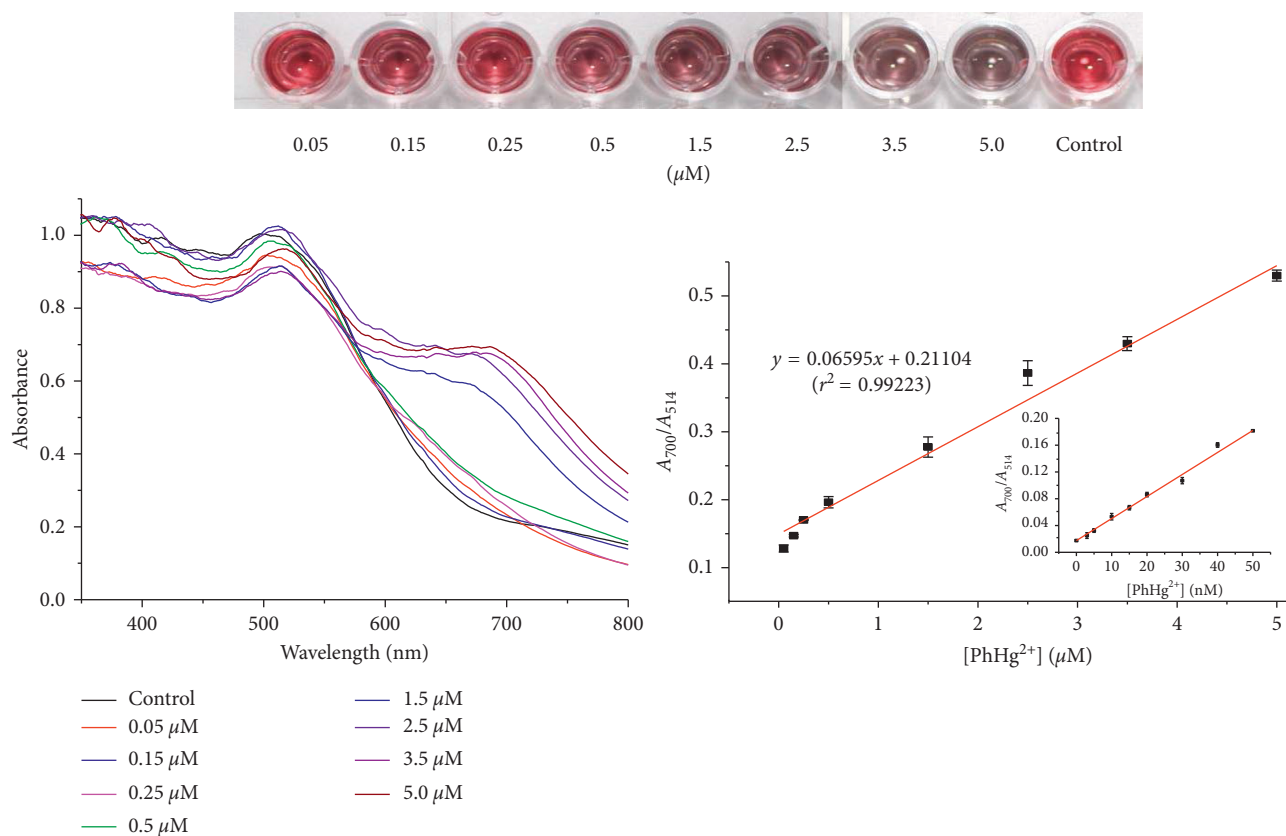
(b)

FIGURE 6: Continued.





(c)



(d)

FIGURE 6: Photographic images, UV-Vis absorption spectra, and absorption ratios ( $A_{700}/A_{514}$ ) of the color change of PEI-AuNPs upon addition of (a)  $\text{Hg}^{2+}$ , (b)  $\text{MeHg}^+$ , (c)  $\text{EtHg}^+$ , and (d)  $\text{PhHg}^{2+}$  with various concentrations (0.05, 0.15, 0.25, 0.5, 1.5, 2.5, 3.5, and 5.0  $\mu\text{M}$  from left to right) in the presence of 300 mM-NaCl. Inset: plot of  $A_{700}/A_{514}$  versus (a)  $\text{Hg}^{2+}$ , (b)  $\text{MeHg}^+$ , (c)  $\text{EtHg}^+$ , and (d)  $\text{PhHg}^{2+}$  ion concentration (0–50 nM).



images and Zetasizer measurements (Figures 1(b) and 1(c)). The color of these PEI-AuNPs was similar to those of label-free AuNPs, but distinct color change occurred from red to dark violet upon addition of  $\text{Hg}^{2+}$  ions. UV-Vis absorption spectra for AuNP, PEI-AuNP, and  $\text{Hg}^{2+}$ -PEI-AuNP solutions are demonstrated in Figure 1(a). Upon addition of  $\text{Hg}^{2+}$  ions, the strong absorption band of PEI-AuNPs at 514 nm was gradually shifted to 700 nm, and a new absorbance band concomitantly increased in intensity upon addition of  $\text{Hg}^{2+}$  ions (Figure 1(a)). When PEI-AuNPs are aggregated, the conduction electrons near their surfaces become delocalized and are shared amongst neighboring particles. As a result, the surface plasmon resonance (SPR) shifts to lower energies, causing the shift of absorption and scattering peaks to longer wavelengths.

**3.2. Selectivity of PEI-AuNPs for  $\text{Hg}^{2+}$  Ions and Related Interference Effects.** The selectivity for PEI-AuNP assay method was tested in  $50 \mu\text{M} \cdot \text{Hg}^{2+}$  and various  $500 \mu\text{M}$  metal cations ( $\text{Zn}^{2+}$ ,  $\text{Cd}^{2+}$ ,  $\text{Cu}^{2+}$ ,  $\text{Cr}^{3+}$ ,  $\text{Pb}^{2+}$ ,  $\text{As}^{3+}$ ,  $\text{Al}^{3+}$ ,  $\text{Mg}^{2+}$ ,  $\text{Co}^{2+}$ ,  $\text{Mn}^{2+}$ ,  $\text{Sn}^{2+}$ ,  $\text{Fe}^{3+}$ ,  $\text{Ge}^{4+}$ ,  $\text{Ni}^{2+}$ ,  $\text{Ga}^{3+}$ ,  $\text{Li}^+$ ,  $\text{Ti}^{4+}$ ,  $\text{K}^+$ ,  $\text{Ba}^{2+}$ , and  $\text{Ca}^{2+}$  ions) and anions ( $\text{F}^-$ ,  $\text{Cl}^-$ ,  $\text{Br}^-$ ,  $\text{SO}_4^{2-}$ ,  $\text{PO}_4^{3-}$ ,  $\text{NO}_2^-$ , and  $\text{NO}_3^-$  ions). The interference by other  $500 \mu\text{M}$  numerous anions and cations for the selectivity of  $\text{Hg}^{2+}$  was further examined. Any metal cations and anions did not induce any color changes except  $\text{Hg}^{2+}$ , as shown in Figure 2(a). UV-Vis absorption spectra of PEI-AuNPs solutions at pH 7,  $50^\circ\text{C}$ , and  $300 \text{ mM} \cdot \text{NaCl}$  concentration were recorded in the presence of various metal cations and anions (Figure 2(b)). The strong absorption band at 700 nm distinctly appeared for  $\text{Hg}^{2+}$ , enabling to discriminate easily from different metal cations and anions. The absorbance ratios ( $A_{700}/A_{514}$ ) of the PEI-AuNPs solution upon addition of each cation and anion were measured to test the selectivity for  $\text{Hg}^{2+}$  ion (Figure 2(c)). The absorbance ratio of PEI-AuNPs solution in the presence of  $\text{Hg}^{2+}$  was  $\sim 11$  times greater than those in the presence of other ions. A high absorbance ratio of  $\text{Hg}^{2+}$ -PEI-AuNPs was attributed to the aggregation of PEI-AuNPs, whereas a low absorbance ratio of PEI-AuNPs in the presence of other ions indicated to keep well-dispersed forms of PEI-AuNPs. Therefore,  $\text{Hg}^{2+}$  ion must be selectively coordinated with a specific site of PEI-AuNPs. The interference effect by other ions in the selectivity of  $\text{Hg}^{2+}$  toward PEI-AuNPs was tested in PEI-AuNP solutions upon addition of  $\text{Hg}^{2+}$  ions mixed with other ions. Other ions did not interfere with determination of  $\text{Hg}^{2+}$ , even though their concentrations were ten times greater than that of  $\text{Hg}^{2+}$ . No metal cations and anions except  $\text{Hg}^{2+}$  perturbed absorption bands at 514 and 700 nm (Figure 2(d)).

**3.3. Binding Sites of PEI to AuNPs and  $\text{Hg}^{2+}$  to PEI-AuNPs.** XPS spectra for PEI-AuNPs and  $\text{Hg}^{2+}$ -PEI-AuNPs were measured to confirm the binding site of  $\text{Hg}^{2+}$  ion to PEI-AuNPs (not shown) [33]. The high-resolution N 1s signal in  $\text{Hg}^{2+}$ -PEI-AuNPs at 406.2 eV showed the binding energy of  $\text{Hg}^{2+}$ -N bonds [34]. Thus, it was found that  $\text{Hg}^{2+}$  ion must be bound to nitrogen atom of PEI.

The binding site of  $\text{Hg}^{2+}$  to PEI was further examined with  $^{13}\text{C}$  NMR spectra for free PEI and PEI bound to  $\text{Hg}^{2+}$

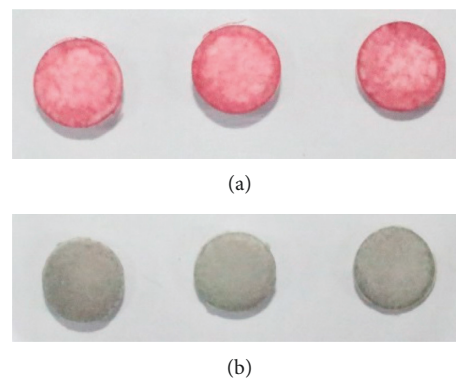


FIGURE 7: (a) Photographic image of the Whatman paper added with PEI-AuNP solution and dried. (b) Photographic image of the Whatman paper added with  $0.1 \text{ ppm} \cdot \text{Hg}^{2+}$  ion solution.

( $\text{Hg}^{2+}$ -PEI) as a model of PEI-AuNPs and  $\text{Hg}^{2+}$ -PEI-AuNPs (Figure 3).  $^{13}\text{C}$  NMR spectra showed that two  $\text{CH}_2$  peaks (peaks 1 and 3) resonating 56.5 ppm and 51.0 ppm in free PEI shifted significantly to 54.5 and 49.8 ppm, respectively, in comparison to those of  $\text{Hg}^{2+}$ -PEI, as shown in Figure 3. The chemical shifts of other peaks changed a little, which indicated that  $\text{Hg}^{2+}$  ions must be coordinated to nitrogen atoms of tertiary amine in PEI [35, 36].

TOF-SIMS spectra for PEI-AuNPs and  $\text{Hg}^{2+}$ -PEI-AuNPs showed an additional evidence for  $\text{Hg}^{2+}$  binding site to PEI-AuNPs (Figure 4). TOF-SIMS spectra of  $\text{Hg}^{2+}$ -PEI-AuNPs provided an additional information for  $\text{Hg}^{2+}$  binding site to PEI-AuNPs. These MS spectra showed the molecular fragments of  $(\text{CH}_2)_2\text{NHg}^{2+}$  ( $m/z$ : 242),  $\text{CH}_2\text{CH}_2(\text{CH}_2)_2\text{NHg}^{2+}$  ( $m/z$ : 270), and  $(\text{CH}_2)_2\text{NHg}^{2+}\text{N}(\text{CH}_2)\text{CH}_2\text{CH}_2$  ( $m/z$ : 298) in  $\text{Hg}^{2+}$ -PEI-AuNPs (Figure 4). These molecular fragments did not appear for PEI-AuNPs, which indicated that  $\text{Hg}^{2+}$  must be coordinated with tertiary nitrogen atoms in PEI [37].

**3.4. Optimum Conditions for PEI-AuNP Probe.** To optimize the sensitivity of the PEI-AuNP probe for  $\text{Hg}^{2+}$ , the probe was tested as functions of pH, temperature, salt concentration, PEI concentration, and reaction time. The absorbance ratios changed as a function of pH, and it was the highest at pH 7 (Figure 5(a)). This optimum pH of the PEI-AuNP probe must be something to do with pKa of tertiary amine and the conformation of PEI [38]. Thus,  $\text{Hg}^{2+}$  must be optimally coordinated to nitrogen elements of PEI in its N-tetrahedral form at pH 7, leading to the highest sensitivity of the probe [39].

The sensitivity of the PEI-AuNP probe for  $\text{Hg}^{2+}$  ions was examined as a function of temperature in the range of  $30\text{--}100^\circ\text{C}$ , and its sensitivity was optimized at  $50^\circ\text{C}$  (Figure 5(b)). Also, the sensitivity of PEI-AuNP probe was monitored as a function of NaCl concentration, and it was optimized at  $300 \text{ mM} \cdot \text{NaCl}$  concentration (Figure 5(c)).

The optimum concentration of PEI conjugated to AuNPs was examined in the presence of  $0.4 \mu\text{g} \cdot \text{mL}^{-1}$   $\text{Hg}^{2+}$  solution,

TABLE 1: Concentrations of  $\text{Hg}^{2+}$  ions measured by the PEI-AuNP colorimetric probe and DMA in tap water, pond water, tuna fish, and bovine serum samples spiked with  $\text{Hg}^{2+}$  ions.

Sample	Content of $\text{Hg}^{2+}$ added to various samples ( $n=7$ )					DMA Detected amount ( $\mu\text{M}$ )
	Added amount ( $\mu\text{M}$ )	Detected amount ( $\mu\text{M}$ )	Coefficient of variation (%)	Recovery (%)	LOD (nM)	
Tap water	0.150	$0.149 \pm 1.53 \times 10^{-4}$	0.102	$99.9 \pm 0.102$	1.72	0.153
	0.500	$0.499 \pm 0.0101$	2.03	$99.9 \pm 2.03$		0.505
Pond water	0.150	$0.150 \pm 6.92 \times 10^{-4}$	0.460	$100.2 \pm 0.461$	1.80	0.156
	0.500	$0.500 \pm 3.41 \times 10^{-3}$	0.682	$100.1 \pm 0.683$		0.504
Tuna fish	0.150	$0.149 \pm 7.09 \times 10^{-4}$	0.473	$99.8 \pm 0.473$	2.00	0.152
	0.500	$0.503 \pm 0.0155$	3.08	$100.6 \pm 3.10$		0.504
Bovine serum	0.150	$0.150 \pm 6.43 \times 10^{-4}$	0.427	$100.1 \pm 0.428$	1.95	0.155
	0.500	$0.503 \pm 7.68 \times 10^{-3}$	1.52	$100.7 \pm 1.53$		0.507

TABLE 2: Analytical results for the detection of  $\text{Hg}^{2+}$  in real citrus leaf samples.

Samples	This method				DMA Average value (nM)
	Average value (nM)	Recovery (%)	RSD (%)	Accuracy (%)	
1	$22.8 \pm 0.34$	101.8	1.54	0.22	22.4
2	$23.9 \pm 0.42$	98.7	1.72	1.29	24.3
3	$23.1 \pm 0.50$	98.1	2.13	1.90	23.5

RSD: relative standard deviation.

TABLE 3: Comparison of previously reported instrumental methods and nanoparticle assay methods proposed for the detection of  $\text{Hg}^{2+}$ .

	Sensing principles	Matrices	LOD	Reference
Instruments				
DMA	—	River sediment, bovine liver, tomato leaves, spinach leaves, sewage sludge, mussel tissue, fish tissue, fish protein	$1.04 \mu\text{M}$	[8]
IC	IC	Tunny fish, oyster, and trumpet	$0.5 \mu\text{M}$	[9]
HPLC	SPE	Tap water, river water, sea water, and coal-washing waste water	14.9 nM	[10]
HPLC	SAX	Drinking water, lake water, river water, tap water, and sea water	0.8 nM	[11]
Functionalized nanoparticles				
AuNRs	Colorimetric	—	14.9 nM	[12]
CNPs	Fluorometric	Tap water and commercial bottled mineral water	10 nM	[13]
AgNPs	Colorimetric	Tap water	1 nM	[14]
AgNPRs	Colorimetric	Lake water and tap water	3.0 nM	[15]
Lysine-AuNPs	Colorimetric	Tap water	2.9 nM	[16]
DDTC-AuNPs	Colorimetric	Drinking water	2.9 nM	[17]
TCA-AuNCs	Colorimetric	Tap water and lake water	0.5 nM	[18]
PEI-AuNPs	Colorimetric	Tap water and pond water	1.72 nM	This study

SPE: solid phase extraction; SAX: strong anion exchange column; DDTC: diethyldithiocarbamate; TCA: thiocyanuric acid.

and the absorbance ratio of UV-Vis spectra as a function of PEI concentration revealed that optimum concentration of PEI was  $\sim 33 \mu\text{M}$  (data not shown).

3.5. Quantitation of  $\text{Hg}^{2+}$ ,  $\text{EtHg}^+$ ,  $\text{MeHg}^+$ , and  $\text{PhHg}^+$  Using the PEI-AuNP Assay Method. The change for color, UV-Vis spectra, and TEM image of the PEI-AuNP probe upon

addition of inorganic ( $\text{Hg}^{2+}$ ) and organic mercury ions ( $\text{MeHg}^+$ ,  $\text{EtHg}^+$ , and  $\text{PhHg}^+$ ) were monitored. The color of PEI-AuNPs changed gradually from red to dark violet as the concentration of mercuric ions increased (Figure 6). Also, the absorbance increases at 700 nm and decreases concomitantly at 514 nm, as the concentration of mercuric ions increases (0.05, 0.15, 0.25, 0.50, 1.5, 2.5, 3.5, and  $5.0 \mu\text{M}$ ) in PEI-AuNPs solutions. The absorbance ratios for concentrations of each

mercuric ion were measured in triplicate. Linear regression analysis of the calibration curve showed a good linearity ( $r^2$  was 0.9817 for  $\text{Hg}^{2+}$ , 0.98009 for  $\text{MeHg}^+$ , 0.98774 for  $\text{EtHg}^+$ , and 0.99223 for  $\text{PhHg}^+$ ) within the linear dynamic range of 0.003–3.0  $\mu\text{M}$ . The limits of detection of this probe in tap, pond water, bovine serum, and tuna fish using this probe were measured as 1.72, 1.80, 2.00, and 1.95 nM, respectively, using  $[3\sigma/\text{slope}]$ .

Paper-type sensor was fabricated, and the present probe solution was dropped to the Whatman paper, and dried it. The color of the Whatman paper turned red (Figure 7(a)), and the functionality of the sensor was tested on water sample containing  $\text{Hg}^{2+}$  ion. When water sample of 0.1 ppm  $\text{Hg}^{2+}$  was added onto the Whatman paper disc, its color turned dark purple (Figure 7(b)). This fact showed this paper disc coated with PEI-AuNP solution can be utilized as a paper-type  $\text{Hg}^{2+}$  sensor.

**3.6. Application of the PEI-AuNP Probe in the Analyses of Real Samples.** To validate the present assay method, the colorimetric responses in real water samples were tested. The tap water, pond water, bovine serum, and tuna fish samples spiked with 0.6 and 1.8  $\mu\text{M}\cdot\text{Hg}^{2+}$  were analyzed using the PEI-AuNP probe and DMA. As shown in Table 1, the analytical results of the proposed probe are nearly identical to those obtained using DMA.  $\text{Hg}^{2+}$  ions in real citrus leaf samples were also determined using both the colorimetric AuNP probe and DMA, as shown in Table 2, and their analytical results are almost the same. Thus, present AuNP-based probe in determination of  $\text{Hg}^{2+}$  ions seemed to be more advantageous than instrumental methods in terms of simplicity, sensitivity, cost, and time.

The previously reported instrumental methods and nanoparticle assay methods for the detection of  $\text{Hg}^{2+}$  ions are compared in Table 3, showing that the colorimetric PEI-AuNP probe offers the lowest LOD for the determination of  $\text{Hg}^{2+}$  ions in aqueous samples.

## 4. Conclusions

A highly sensitive and selective colorimetric probe to determine  $\text{Hg}^{2+}$  ions was developed using AuNPs conjugated with branched polyethyleneimine. The sensing mechanism of this colorimetric probe was originated from the aggregation of PEI-AuNPs in the presence of  $\text{Hg}^{2+}$ , and the  $\text{Hg}^{2+}$  ion was found to be selectively coordinated by nitrogen element of PEI conjugated with AuNPs. This method offers simple, highly sensitive, highly selective, and cost-efficient on-site monitoring of the  $\text{Hg}^{2+}$  ion, allowing the detection of concentrations as low as 1.72 nM to be visually achieved within 40 min.

## Conflicts of Interest

The authors declare that there are no conflicts of interest regarding the publication of this paper.

## Authors' Contributions

Kyung Min Kim and Yun-Sik Nam equally contributed to this work.

## Acknowledgments

This research was financially supported by Korea Institute of Science and Technology (2E27070) and the Korea Ministry of Environment (2016000160008) as "Public Technology Program based on Environmental Policy."

## References

- [1] J. A. Cowan, *Inorganic Biochemistry: An Introduction*, Wiley-VCH, Weinheim, Germany, 1997.
- [2] M. Gibb and K. G. O'Leary, "Mercury exposure and health impacts among individuals in the artisanal and small-scale gold mining community: a comprehensive review," *Environmental Health Perspectives*, vol. 122, no. 7, pp. 667–672, 2014.
- [3] J. D. Park and W. Zheng, "Human exposure and health effects of inorganic and elemental mercury," *Journal of Preventive Medicine and Public Health*, vol. 45, no. 6, pp. 344–352, 2012.
- [4] Y. Fang, X. Sun, W. Yang et al., "Concentrations and health risks of lead, cadmium, arsenic, and mercury in rice and edible mushrooms in China," *Food Chemistry*, vol. 147, pp. 147–151, 2014.
- [5] Y. S. Hong, Y. M. Kim, and K. E. Lee, "Methylmercury exposure and health effects," *Journal of Preventive Medicine and Public Health*, vol. 45, no. 6, pp. 353–363, 2012.
- [6] J. G. Dórea, M. Farina, and J. B. Rocha, "Toxicity of ethylmercury (and Thimerosal): a comparison with methylmercury," *Journal of Applied Toxicology*, vol. 33, no. 8, pp. 700–711, 2013.
- [7] D. A. Geier, B. S. Hooker, J. K. Kern, P. G. King, L. K. Sykes, and M. R. Geier, "A dose-response relationship between organic mercury exposure from thimerosal-containing vaccines and neurodevelopmental disorders," *International Journal of Environmental Research and Public Health*, vol. 11, no. 9, pp. 9156–9170, 2014.
- [8] C. C. Windmoller, N. C. Silva, P. H. M. Andrade, L. A. Mendes, and C. M. do Valle, "Use of a direct mercury analyzer® for mercury speciation in different matrices without sample preparation," *Analytical Methods*, vol. 9, pp. 2159–2167, 2017.
- [9] Q. Liu, "Determination of mercury and methylmercury in seafood by ion chromatography using photo-induced chemical vapor generation atomic fluorescence spectrometric detection," *Microchemical Journal*, vol. 95, no. 2, pp. 255–258, 2010.
- [10] Y. Yin, M. Chen, J. Peng, J. Liu, and G. Jiang, "Dithizone-functionalized solid phase extraction–displacement elution–high performance liquid chromatography–inductively coupled plasma mass spectrometry for mercury speciation in water samples," *Talanta*, vol. 81, no. 4–5, pp. 1788–1792, 2010.
- [11] H. Cheng, C. Wu, L. Shen, J. Liu, and Z. Xu, "Online anion exchange column preconcentration and high performance liquid chromatographic separation with inductively coupled plasma mass spectrometry detection for mercury speciation analysis," *Analytica Chimica Acta*, vol. 828, pp. 9–16, 2014.
- [12] T. Placido, G. Aragay, J. Pons, R. Comparelli, M. L. Curri, and A. Merkoçi, "Ion-directed assembly of gold nanorods: a strategy for mercury detection," *ACS Applied Materials & Interfaces*, vol. 5, no. 3, pp. 1084–1092, 2013.
- [13] Y. Guo, Z. Wang, H. Shao, and X. Jiang, "Hydrothermal synthesis of highly fluorescent carbon nanoparticles from sodium citrate and their use for the detection of mercury ions," *Carbon*, vol. 52, pp. 583–589, 2013.

- [14] L. Li, L. Gui, and W. Li, "A colorimetric silver nanoparticle-based assay for Hg(II) using lysine as a particle-linking reagent," *Microchimica Acta*, vol. 182, pp. 1977–1981, 2015.
- [15] N. Chen, Y. Zhang, H. Liu et al., "High-performance colorimetric detection of Hg<sup>2+</sup> based on triangular silver nanoparticles," *ACS Sensors*, vol. 1, no. 5, pp. 521–527, 2016.
- [16] G. Sener, L. Uzun, and A. Denizli, "Lysine-promoted colorimetric response of gold nanoparticles: a simple assay for ultrasensitive mercury(II) detection," *Analytical Chemistry*, vol. 86, no. 1, pp. 514–520, 2014.
- [17] L. Chen, J. Li, and L. Chen, "Colorimetric detection of mercury species based on functionalized gold nanoparticles," *ACS Applied Materials & Interfaces*, vol. 6, no. 18, pp. 15897–15904, 2014.
- [18] Z. Chen, C. Zhang, H. Ma et al., "A non-aggregation spectrometric determination for mercury ions based on gold nanoparticles and thiocyanuric acid," *Talanta*, vol. 134, pp. 603–606, 2015.
- [19] W. J. Song, J. Z. Du, T. M. Sun, P. Z. Zhang, and J. Wang, "Gold Nanoparticles capped with polyethyleneimine for enhanced siRNA delivery," *Small*, vol. 6, no. 2, pp. 239–246, 2010.
- [20] Z. Yuan, N. Cai, Y. Du, Y. He, and E. S. Yeung, "Sensitive and selective detection of copper ions with highly stable polyethyleneimine-protected silver nanoclusters," *Analytical Chemistry*, vol. 86, no. 1, pp. 419–426, 2014.
- [21] Y. Liu, Z. Li, J. Liu, L. Xu, and X. Liu, "An unusual red-to-brown colorimetric sensing method for ultrasensitive silver(I) ion detection based on a non-aggregation of hyperbranched polyethylenimine derivative stabilized gold nanoparticles," *Analyst*, vol. 140, no. 15, pp. 5335–5343, 2015.
- [22] V. V. Kumar, M. K. Thenmozhi, A. Ganesan, S. S. Ganesan, and S. P. Anthony, "Hyperbranched polyethyleneimine-based sensor of multiple metal ions (Cu<sup>2+</sup>, Co<sup>2+</sup> and Fe<sup>2+</sup>): colorimetric sensing via coordination or AgNP formation," *RCS Advances*, vol. 5, pp. 88125–88132, 2015.
- [23] M. Li, Y. Li, X. Huang, and X. Lu, "Captopril-polyethyleneimine conjugate modified gold nanoparticles for co-delivery of drug and gene in anti-angiogenesis breast cancer therapy," *Journal of Biomaterials Science, Polymer Edition*, vol. 26, no. 13, pp. 813–827, 2015.
- [24] N. D. Huston, B. C. Attwood, and K. G. Scheckel, "XAS and XPS characterization of mercury binding on brominated activated carbon," *Environmental Science & Technology*, vol. 41, no. 5, pp. 1747–1752, 2007.
- [25] J. B. Lindén, M. Larsson, S. Kaur et al., "Polyethyleneimine for copper absorption II: kinetics, selectivity and efficiency from seawater," *RSC Advances*, vol. 5, pp. 51883–51890, 2015.
- [26] J. D. S. Newman and G. J. Blanchard, "Formation of gold nanoparticles using amine reducing agents," *Langmuir*, vol. 22, no. 13, pp. 5882–5887, 2006.
- [27] J. Bell, E. Climent, M. Hecht, M. Buurman, and K. Rurack, "Combining a Droplet-based microfluidic tubing system with gated indicator releasing nanoparticles for mercury trace detection," *ACS Sensors*, vol. 1, no. 4, pp. 334–338, 2016.
- [28] X. Cui, L. Zhu, Y. Hou, P. Wang, Z. Wang, and M. Yang, "A fluorescent biosensor based on carbon dots-labeled oligodeoxyribonucleotide and graphene oxide for mercury (II) detection," *Biosensors and Bioelectronics*, vol. 63, pp. 506–512, 2015.
- [29] M. J. Rak, N. K. Saadé, T. Friščić, and A. Moores, "Mechanosynthesis of ultra-small monodisperse amine-stabilized gold nanoparticles with controllable size," *Green Chemistry*, vol. 16, pp. 86–89, 2014.
- [30] C. Lin, K. Tao, D. Hua, Z. Ma, and S. Zhou, "Size Effect of gold nanoparticles in catalytic reduction of *p*-nitrophenol with NaBH<sub>4</sub>," *Molecules*, vol. 18, no. 10, pp. 12609–12620, 2013.
- [31] C. Deraedt, L. Salmon, S. Gatard et al., "Sodium borohydride stabilizes very active gold nanoparticle catalysts," *Chemical Communications*, vol. 50, pp. 14194–14196, 2014.
- [32] S. K. Ghosh and T. Pal, "Interparticle coupling effect on the surface plasmon resonance of gold nanoparticles: from theory to applications," *Chemical Reviews*, vol. 107, no. 11, pp. 4797–4862, 2007.
- [33] M. Min, L. Shen, G. Hong et al., "Micro-nano structure poly(ether sulfones)/poly(ethyleneimine) nanofibrous affinity membranes for adsorption of anionic dyes and heavy metal ions in aqueous solution," *Chemical Engineering Journal*, vol. 197, pp. 88–100, 2012.
- [34] F. F. Tao, "Design of an *in-house* ambient pressure AP-XPS using a bench-top X-ray source and the surface chemistry of ceria under reaction conditions," *Chemical Communications*, vol. 48, pp. 3812–3814, 2012.
- [35] D. R. Holycross and M. Chai, "Comprehensive NMR studies of the structures and properties of PEI polymers," *Macromolecules*, vol. 46, no. 17, pp. 6891–6897, 2013.
- [36] W. Y. Seow, K. Liang, M. Kurisawa, and C. A. E. Hauser, "Oxidation as a facile strategy to reduce the surface charge and toxicity of polyethyleneimine gene carriers," *Bio-macromolecules*, vol. 14, no. 7, pp. 2340–2346, 2013.
- [37] D. Schaubroeck, Y. Vercammen, L. V. Vaeck, E. Vanderleyden, P. Dubruel, and J. Vanfleteren, "Surface characterization and stability of an epoxy resin surface modified with polyamines grafted on polydopamine," *Applied Surface Science*, vol. 303, pp. 465–472, 2014.
- [38] K. A. Curtis, D. Miller, P. Millard, S. Basu, F. Horkay, and P. L. Chandran, "Unusual salt and pH induced changes in polyethylenimine solutions," *PLoS One*, vol. 11, no. 9, Article ID e0158147, 2016.
- [39] J. Gaffney and N. Marley, "In-depth review of atmospheric mercury: sources, transformations, and potential sinks," *Energy and Emission Control Technologies*, vol. 2, pp. 1–21, 2014.





Hindawi

Submit your manuscripts at  
[www.hindawi.com](http://www.hindawi.com)

